Received: 14 October 2022 | Accepted: 5 January 2023

DOI: 10.1111/opo.13095

OPO THE COLLEGE OF OPTOMETRISTS

ORIGINAL ARTICLE

Conformation of the anterior segment in human myopia

Hetal Buckhurst[1] | **Bernard Gilmartin**[2] | **Robert Cubbidge**[3] | **Nicola S. Logan**[2]

[1]Faculty of Health, Plymouth of University, Plymouth, UK

[2]School of Optometry, Aston University, Birmingham, UK

[3]ABDO College, Canterbury, UK

Correspondence
Hetal Buckhurst, Faculty of Health, Plymouth of University, Plymouth, UK.
Email: hetal.buckhurst@plymouth.ac.uk

Abstract

Purpose: Topography of the *in vivo* anterior segment is of relevance in understanding its role in myopia and in the development of ocular surgical procedures. Using 3D magnetic resonance (MR) images of the human eye, regional variations in surface area (SA) and bulbosity of four anterior segment regions were investigated in association with refractive status (Rx), axial length (AL) and total ocular volume (OV).

Methods: T2-weighted ocular MR images from 43 adults aged 18–40 years (mean ± SD; 28.65 ± 6.20) comprising 20 non-myopes (≥−0.50) 0.57 ± 1.38 and 23 myopes (<−0.50) −6.37 ± 4.23 MSE (D) were collected. 2D representations of each quadrant (superior-temporal [ST], superior-nasal [SN], inferior-temporal [IT] and inferior-nasal [IN]) of the anterior section (3.5–9 mm) were fitted with second-order polynomials. Polynomials were integrated and rotated about the *x*-axis to generate SA; dividing the SA by 4 provided relative quadrantial SA. The x^2 coefficient provides indices of bulbosity. OV was derived from the 3D MRI scans. Rx and AL were measured using cycloplegic autorefraction and the Zeiss IOLMaster, respectively. One- and two-way repeated-measures ANCOVAs tested differences in SA and bulbosity for Rx, gender, ethnicity and age. Pearson's correlation coefficient tested the relationship between MRI-derived metrics and biometry.

Results: Significant differences in SA were observed between quadrants ($p < 0.001$) with differences between ST versus IN, IN versus IT and SN versus IT. An interaction effect ($p = 0.01$) for Rx suggested smaller temporal (ST and IT) and larger nasal (SN and IN) SA in myopes. AL and myopic Rx were negative correlated ($p < 0.05$) with SA at IN, SN and IT. OV was significantly associated with SA at ST. Bulbosity showed no regional differences nor an effect of AL or Rx.

Conclusion: Significant regional variation in SA exists across the anterior segment that is modulated by Rx and AL. It is unclear whether these structural characteristics are a precursor or consequence of myopia and may warrant investigation when developing biomechanical interventions.

KEYWORDS
anterior segment shape, MRI, myopia, surface area and eye shape

INTRODUCTION

While the posterior structural changes that accompany myopia are well established both clinically[1,2] and histopathologically,[3,4] it is unclear whether more subtle biomechanical changes to the sclera manifest across the anterior segment.[5–9] Although variation in anterior scleral thickness with myopia has not been widely observed,[8,10,11] more recently, thinning has been noted at discrete points along the inferior,[12,13] temporal and nasal meridia.[13] Dynamic changes to the anterior sclera in eyes with myopia have also been reported; changes in scleral shape[14] and thinning[15]

were observed to be greater during accommodation in myopes, while Niyazamand et al.[5] reported that high myopes exhibited greater thickening with increasing levels of convergence. Posterior and equatorial eye shape are also known to alter in myopia,[16,17] but few studies that assessed the anterior surface shape suggested myopic eyes to be less asymmetric[6,18] and demonstrated greater nasal sagittal height.[18] Observations of larger anterior chamber depth and flatter corneal curvature in myopic eyes suggest a putative involvement of the anterior segment in myopia development and progression.[19–21]

An accurate depiction of the anterior segment shape is of relevance to many areas of clinical work including scleral contact lens design,[22] intraocular lens geometry,[23,24] transscleral drug delivery,[25] intravitreal injections,[26] scleral collagen cross-linking,[27,28] as well as any surgical procedures involving the anterior sclera.[29,30] The accessibility of the anterior aspect of the eye is a major advantage, but technical challenges related to imaging through the sclera and determining suitably valid and sensitive metrics for identifying physical alterations *in vivo* pose another difficulty. Several investigators have attempted to model the anterior scleral shape via corneoscleral topography[5,18,22,31] and optical coherence tomography (OCT),[18,32,33] but these are limited to assessment of only the exposed scleral and corneal surfaces and imaging along discrete meridia and depth.[22] Restrictions as to how far posteriorly the *in vivo* anterior segment can be imaged with OCT has constrained assessment of the sagittal height to 15-mm chord lengths[22] and thickness measurements to 6 mm posterior to the scleral spur.[8,13] Moreover, effects of refractive distortion and tissue curvature and tilt further compound OCT imaging.[34]

To evaluate comprehensively the topography of the anterior segment, an assessment of the three-dimensional (3D) eye shape *in vivo* is valuable.[35,36] Magnetic resonance imaging (MRI) is based on high-contrast delineation of the vitreo-retinal interface, and thus provides a determination of the internal surface of the eye. As an *in vivo* method of non-contact imaging, MRI allows depiction and investigation of the internal ocular globe. The utility of MRI in humans in evaluating ocular features such as retinal and posterior vitreous chamber shape,[18,37] linear dimensions,[38,39] surface area (SA) and curvature[40,41] and ocular and orbital volume.[42–44] has been demonstrated. Despite its use in these studies,[45,46] application of MRI has not been extended into the evaluation of structural characteristics within the anterior segment of the globe.

It is well documented that myopia results from the anterior segment components failing to compensate for the concurrent growth of the posterior vitreous chamber.[47,48] Specifically, the observation that the ciliary muscle has been identified as restricting the anterior processes governing crystalline lens flattening with axial length (AL) expansion may be the basis for myopic growth.[49,50] MR imaging of the anterior segment provides a unique opportunity to characterise the internal morphometry of the anterior segment without the effects of the overlying tissues nor the constraints of the anterior–posterior limits of OCT and topography. To encompass the region of the ciliary muscle[43,50] as well as previous work pertaining to the anterior segment structure,[6–9,18,23,24] a novel metric to assess MRI-derived SAs and bulbosity of four anterior segment quadrants was assessed. The influence of refractive status as well as associated AL and ocular volume (OV) on these structural characteristics was also investigated.

Key points

- Topography of the *in vivo* anterior segment is of relevance in understanding its role in myopia and in the development of ocular surgical procedures.
- Using 3D magnetic resonance images of the human eye, regional variations in surface area and bulbosity of four anterior segment regions were investigated.
- Significant regional variation in surface area exists across the anterior segment that are modulated by refractive error and axial length.

METHOD

Forty-three young adult subjects were scanned using a whole body MRI scanner (3-Tesla Trio, Siemens, siemens-healthineers.com). Ethical approval was obtained from Aston University Ethics Committee and the study was performed according to the tenets of the Declaration of Helsinki. Written informed consent was obtained from each subject prior to the commencement of the study. Eligibility to take part in the study was confirmed after subjects completed a screening questionnaire. Exclusion criteria were as follows: previous history of ocular surgery, trauma or pathology, ocular medication, astigmatism >1.75 D as well as standard criteria[51] for MR scanning. Individuals suffering from connective tissue–related disorders were also excluded due to their known effect on collagen composition and, hence, its probable effect on scleral biomechanics and eye structure.

Acquisition of MR images

Magnetic resonance images were acquired using an eight-channel phased-array head coil, which allows simultaneous scanning of both eyes with a high signal-to-noise ratio. T2- weighted scans were obtained using an imaging protocol that allowed high-definition delineation of the ocular surfaces. These scans were performed using a protocol reported previously.[17,42] Subsequently, the T2-weighted MR images (voxel thickness of $0.5 \times 0.5 \times 1.0$ mm) produced by

this sequencing were optimised to allow discrimination of the eye's fluid-filled chambers from the rest of the head scan. Scanning required a distance refractive correction as subjects were asked to fixate on a distance target viewed through an angled mirror mounted on the head coil; any subjects who required such a refractive correction were fitted with best-sphere daily disposable contact lenses to facilitate accurate fixation. The average scanning time was 5 min and 40 s.

Analysis of MR images

Magnetic resonance images were analysed using a specially modified version of the freeware software, *mri3dX*.[17,52] Analysis of the T2-weighted image voxels was conducted as per previous work to produce 3D depictions of the eye shape.[42,43,52] Vector co-ordinates of the 3D surface polygons were designated as superior-temporal (ST), superior-nasal (SN), inferior-temporal (IT) and inferior-nasal (IN) to determine the regional conformation of the globe. These divisions are based on a standardised co-ordinate system where the longitudinal axis of symmetry is projected from a line connecting the geometric centre of the eye to the anterior corneal pole. Although the procedure cannot account fully for the discrepancy between the visual and optical axis (i.e., angle alpha), this discrepancy can be considered relatively small for anterior regions of the globe.

To illustrate the morphological features of the globe, the 3D array of polygons was then collapsed to provide a 2D representation of each quadrant. Data were extracted initially for 15%–100% along the AL for all quadrants; 15% (approx. 3.5 mm posterior to the cornea apex) along the AL allows avoidance of the cornea and assessment of the globe from beyond the corneo-limbal junction while 100% denotes the most posterior aspect of the eye (Figures 1 and 2). This technique provides good correlation with partial coherence interferometry measurement of AL and allows repeatable and reproducible results.[52]

To encapsulate the entirety of this region of special interest, the anterior section lies between ~3.5 and 9 mm, equivalent to approximately 15%–40% along the AL (Figure 2). A second-order polynomial (Equation 1) was fitted to each quadrant for this range (Figure 2). As AL is used as the reference for extracting the 15%–100% range of MRI data, inter-subject variability in AL influences the width of this range and, hence, affects the size of the anterior region (15%–40%) of interest. The study protocol presently adopted controlled, in part, for this source of error. Since the anterior 3.5 mm (15% along the AL) is likely to vary with AL, maintaining a constant end point at 9 mm (i.e., 40% along the AL) ensured that the extent of the region assessed remained relatively constant between subjects.

Surface area was generated by integrating and rotating the second-order polynomial about the *x*-axis. Dividing the segment area by four provided a measure of the relative SA for each quadrant (Equation 2). The coefficient of

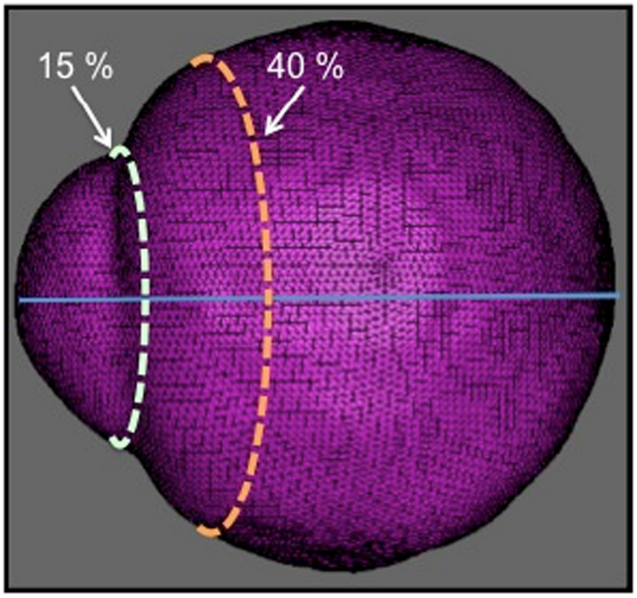

FIGURE 1 Diagrammatic depiction of the 15%–40% axial length range assessed.

the x^2 polynomial offers a measure of the bulbosity of each respective quadrant.

$$y = ax^2 + bx + c \tag{1}$$

The values *a*, *b* and *c* represent coefficient values for the polynomial.

$$S = \frac{\pi}{32a^2}\left[t\sqrt{1+t^2}\left(2t^2+4\left(4ac-b^2\right)\right) + \left(4\left(4ac-b^2\right)-1\right)\ln\left(t+\sqrt{t^2+1}\right)\right]_{t_1}^{t_2} \tag{2}$$

where $t_1 = b + 2al_1$, $t_2 = b - 2al_2$ and SA represents surface area.

The values *a*, *b* and *c* correspond to the polynomial equation values of $y = ax^2 + bx + c$.

The values l_1 and l_2 (in mm) correspond to the respective 15% and 40% *x*-axis values.

Biometric measurements

Refractive error was determined after inducing cycloplegia in each eye using 1 drop of tropicamide HCl 1% (Minims®, bausch.co.uk). Sufficient cycloplegia was designated as an amplitude of accommodation <2D. Objective measurements of the refractive error and central corneal curvature were determined with an infrared, binocular, open-view autorefractor/keratometer (Shin-Nippon SRW-5000, grandseiko.com). Five measurements were taken from each eye, which were averaged and converted to mean spherical error (MSE) (sphere power + 0.5 × cylinder power) and central corneal curvature (mm) readings. AL and anterior chamber

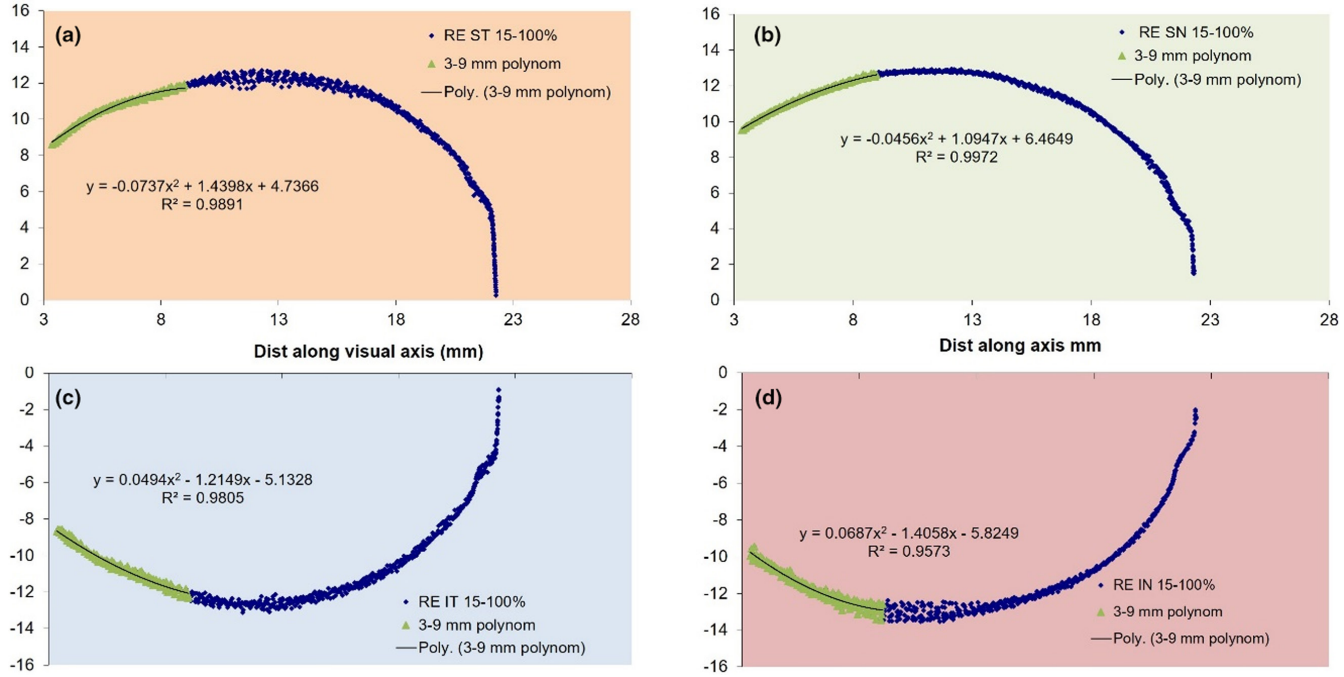

FIGURE 2 The profile of the right eye of subject 10. Data along 15%–100% (blue) and 15%–40% (green) along the visual axis plotted for (a) superior-temporal, (b) superior-nasal, (c) inferior-temporal and (d) inferior-nasal. The second-order polynomial fit for the 15%–40% range for each quadrant is also presented.

depth measurements were taken with the IOLMaster 500 (Carl Zeiss Meditec, Inc., meditec.zeiss.com). Five separate measurements were averaged for AL, whereas a single-capture shot automatically generated and averaged five measurements of anterior chamber depth.

Statistical analysis

Statistical evaluation was performed using SPSS version 25 for Windows (ibm.com) and Microsoft Excel (Microsoft.com). Only data from the right eye (RE) were analysed. Multiple two-way mixed repeated-measures analysis of covariance (ANCOVA) were performed to test for an effect of the between-subject factors: refractive status (myopes and non-myopes), gender, ethnicity (British White [BW] and British South-Asian [BSA]) and age (years) grouping ([18 > to ≤ 29] [>29 to ≤ 40]), on the within-subject factor SAs and bulbosity, while controlling for the covariate factor AL. Additionally, Pearson's correlation coefficient was calculated to test the relationship between SAs and ocular biometry parameters (AL, OV, ACD, mean corneal curvature) for the whole subject group and then separately for the myopic and non-myopic subgroups. For all statistical tests, a p-value of <0.05 was taken as the criterion for statistical significance.

RESULTS

Surface area and bulbosity were assessed in 43 healthy individuals (Table 1).

TABLE 1 Descriptive data (mean ± SD) for non-myopic (n = 20) and myopic (n = 23) subjects.

	Non-myopes (MSE ≥ −0.50 D) n **= 20**	**Myopes (MSE < −0.50 D)** n **= 23**
Gender (male:female)	10:10	6:17
Ethnicity (BSA:BW)	9:11	10:13
Age (years)		
Mean ± SD	29.25 ± 6.97	28.13 ± 5.55
Range	19 to 40	20 to 40
MSE (D)		
Mean ± SD	0.57 ± 1.38	−6.37 ± 4.23
Range	−0.50 to +4.38	−20.50 to −0.75
Axial length (mm)		
Mean ± SD	23.37 ± 0.63	25.77 ± 1.27
Range	21.75 to 24.45	23.33 to 28.32
Ocular volume (mm^3)		
Mean ± SD	7524 ± 757	8744 ± 1132
Range	5036 to 8464	6724 to 11,777

Abbreviations: BSA, British South-Asian; BW, British White, MSE, mean spherical equivalent; SD, standard deviation.

Surface area

Axial length was a significant covariate of SA ($F_{1,41}$ = 4.96, p = 0.03); hence, its effect was controlled on subsequent analysis. Significant differences were observed between

TABLE 2 Right eye surface areas of each quadrant (mm^2) for all subjects.

Quadrant	Mean ± SD	Min	Max
ST	106.07 ± 5.70	93.50	115.78
IN	109.74 ± 7.67	85.66	120.24
SN	108.46 ± 5.63	91.04	121.09
IT	104.14 ± 5.62	90.25	116.75

Abbreviations: IN, inferior-nasal; IT, inferior temporal; SN, superior nasal; ST, superior-temporal.

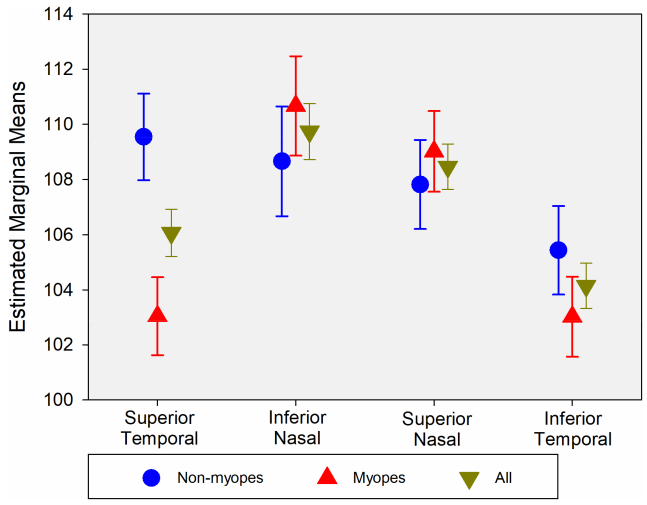

FIGURE 3 Estimated marginal means (± standard error bars) for all four quadrants in the non-myopic group, myopic groups and for all subjects. Estimated marginal means provide the adjusted means after controlling for the covariate axial length for each group hence the effect of axial length was statistically removed.

quadrants ($F_{2.314,94.877} = 12.49$, $p < 0.001$), with IN showing the largest SA and IT the smallest (Table 2). Bonferroni post-hoc test revealed statistically significant differences between ST versus IN, IN versus IT and SN versus IT.

Analysis showed no main effect for refractive status ($F_{1,40} = 0.43$, $p = 0.52$). However, a significant interaction effect was noted between refractive status and regional differences ($F_{2.412,96.498} = 4.27$, $p = 0.01$) suggesting smaller temporal (ST and IT) and larger nasal (SN and IN) SAs in myopes (Table 2 and Figure 3). Neither gender ($F_{1,40} = 0.08$, $p = 0.78$), ethnicity ($F_{1,40} = 0.06$, $p = 0.81$) nor age grouping ($F_{1,40} = 0.86$, $p = 0.36$) showed a significant effect on SA.

Correlates of surface area

For the combined myopic and non-myopic groups, (Table 3a) as well as the separate myopic group (Table 3b), a more myopic refractive error and longer AL were negatively associated with SAs for SN, IN and IT (Table 3a and b). In contrast, this relationship was not observed in the non-myopic group (Table 3c). Although ST SA showed no association with refractive error or AL, it was the only region to show a strong positive association with OV for all groups (Table 3a–c). Among the combined group, mean corneal curvature was positively associated with SAs in the SN, IN and IT quadrants but only in the IT and SN regions for the myopic and non-myopic groups, respectively. No relationship was found between ACD and SAs.

Quadrant bulbosity

The curvature for each region was represented as bulbosity and indexed by the x^2 coefficient of the second-order polynomial over the ≈3.5–9.0 mm section along the axial length (Table 4). Bulbosity failed to show any significant regional differences ($F_{3,123} = 0.88$, $p = 0.45$). None of the following parameters showed any significant effect on bulbosity: axial length ($F_{1,41} = 0.78$, $p = 0.38$), refractive status ($F_{1,40} = 0.03$, $p = 0.87$), gender ($F_{1,40} = 2.02$, $p = 0.16$), ethnicity ($F_{1,40} = 0.03$, $p = 0.86$) and age group ($F_{1,40} = 0.70$, $p = 0.40$).

DISCUSSION

This study is the first to explore the utility of MRI-derived measures of anterior segment SA and bulbosity in eyes of different refractive groups. Notably, these novel metrics provide an evaluation of the internal shape of the anterior segment rather than the external surface, thus mitigating the effects of overlying tissues such as the sclera, episclera, Tenon's capsule and conjunctiva. Regional differences in the SA between the ST versus IN, IN versus IT and SN versus IT quadrants were observed. Interestingly, other than IT versus IN, the SA differences seem to lie between the diagonal quadrants, that is, ST versus IN and SN versus IT, suggesting that most adjacent regions, both horizontally and vertically, are congruent. Anterior scleral shape is known to demonstrate rotational asymmetry, with the sagittal height of the temporal sclera being greater than the nasal and the superior region larger than the inferior.[22,53] The insertion site of the extraocular muscles may influence such structural characteristics.[32,33,54] For the temporal (7.0 mm) and superior (7.5 mm) meridia, the distance from the limbus to the insertion points is larger than for the nasal (5.5 mm) and inferior (6.5 mm) meridia.[55,56] It is possible that different biomechanical forces generated by the extraocular muscles across the various meridia may result in regional disparity in anterior segment growth. Heterogeneity of the internal dimensions of the anterior segment has also been observed previously in regards to the magnitude of the vertical and horizontal meridia.[23,24,57] Inconsistency in the internal dimensions of the anterior eye is likely to affect the overall conformation of the anterior segment and may further explain the variation in SAs found here. Such observations suggest that the anterior eye fails to exhibit the commonly assumed spherical shape, but, in fact, shows considerable regional variation in its morphometry.

TABLE 3 Univariate correlations (Pearson coefficients) between regional surface area and ocular biometrics: (a) combined group (both myopic and non-myopic subjects) (b) only myopes ($n = 23$) and (c) only non-myopic subjects ($n = 20$).

	ST	SN	IN	IT
(a)				
SN	ns			
IN	ns	0.67**		
IT	0.41**	0.59**	0.74**	
Refractive error	ns	0.39**	0.63**	0.46**
Axial length	ns	−0.33*	−0.52**	−0.31*
Ocular volume	0.45**	ns	ns	ns
Mean corneal curvature	ns	0.37*	0.40*	0.51**
(b)				
SN	ns			
IN	ns	0.63**		
IT	ns	0.54**	0.77*	
Refractive error	ns	0.59**	0.75**	0.63*
Axial length	ns	−0.58**	−0.61**	−0.44*
Ocular volume	0.56**	ns	ns	ns
Mean corneal curvature	ns	ns	ns	0.44*
(c)				
SN	ns			
IN	ns	0.78**		
IT	ns	0.51*	0.66**	
Refractive error	ns	ns	ns	ns
Axial length	ns	ns	−0.52**	ns
Ocular volume	0.45**	ns	ns	0.47*
Mean corneal curvature	ns	0.53*	ns	ns

Abbreviations: IN, inferior-nasal; IT, inferior-temporal; SN, superior-nasal; ST, superior-temporal.

*$p < 0.05$, **$p < 0.001$, ns, non-significant.

TABLE 4 Right eye bulbosity represented as the X^2 (coefficient of the second-order polynomials) for each quadrant.

Quadrant	Mean ± SD	Min	Max
X^2 ST	0.08 ± 0.02	0.04	0.12
X^2 IN	0.07 ± 0.02	0.04	0.12
X^2 SN	0.08 ± 0.02	0.04	0.15
X^2 IT	0.07 ± 0.02	0.04	0.14

Abbreviations: IN, inferior-nasal; IT, inferior-temporal; SN, superior-nasal; ST, superior-temporal.

Measurements of the internal conformation may provide a more accurate depiction of growth changes in the myopic eye, which may be a precursor to the observed external scleral shape[6,18] and thickness changes.[12,13] Refractive status was found to have a significant interaction with the regional differences, with smaller temporal and larger nasal SA in myopic eyes. Aside from the ST quadrant, all SAs demonstrated reduction with longer AL and myopic refractive error. It is unclear whether these structural characteristics are a precursor to or a consequence of myopia. There is little evidence in humans to suggest a genetic or environmental factor that may result in such asymmetry with myopia. Differential levels of anatomical restriction offered by the medial and lateral walls during ocular expansion anteriorly, especially near the orbital margin, may partly explain the findings.[58,59] Assuming a constant tissue volume,[60] the smaller SA with increasing AL and myopic refraction may be a subsequent effect of the predominant equatorial and posterior expansion,[17,61,62] which may lead to reduced tissue mass across the anterior regions. The possible propensity for greater globe expansion temporally[63–65] may partly explain why the temporal SA was smaller in myopic eyes. The ST SA uniquely failed to show any association with AL and refraction but demonstrated a consistent, positive relationship with OV, suggesting that this region may be a better indicator of overall globe expansion rather than longitudinal axial growth. Interestingly, the ST quadrant was observed to have the largest retinal SA and the higher incidence of retinal breaks.[41,66] Nagra et al.[44] noted that inter-quadrant differences in the retinal SA existed independent of AL, suggesting that the susceptibility for retinal tears may be more associated with the inter-quadrant differences rather than the absolute magnitude of the retinal surface. It is unclear how the anterior and posterior SA are related, but a biomechanical association may exist which might be modulated differently in myopic eyes.

Despite the findings of regional variation in anterior segment SA, no significant differences were observed between the bulbosity of different quadrants. Bulbosity is an index of the degree of protrusion of a particular element of shape, and hence, is independent of SA and volume. The present study did not assess curvature differences per se since bulbosity is a characteristic of curvature. Visualising the configuration of the anterior eye as an ellipse, having the same vertex curvatures yet different horizontal and vertical dimensions, with asphericity quantified as Q values may help to understand the dissociation with SA. Therefore, with regards to bulbosity, it is possible that anatomical constraints imposed by the surrounding tissue ensure uniformity between the different quadrants assessed. These observations suggest that despite the SA reducing with increasing AL, the actual bulbosity of the quadrant remains constant. Topographic observations of a more symmetrical anterior segment in myopic eyes support these findings.[5,18] Neither ethnicity, gender nor age group were found to have a significant influence on SA and bulbosity.

There are several limitations to this study. The MR image analysis protocol used here provides quadrant reference points based on the geometric (optical) axis, rather than the visual axis. The discrepancy between these two axes is known as angle α. While this angle is present along both the horizontal and vertical meridia, its magnitude is smaller vertically. Angle α is notoriously difficult to assess and

account for[67,68] but it can be assumed that for the anterior segment region assessed in this study, its effects should be minimal. Inter-subject variability in AL is likely to influence the initial 15%–100% of the reference data set extracted to determine the size of the anterior segment region (15%–40%). Although a fixed end point comprising 40% of the AL was used, there is a likelihood that the size of the anterior portion varied with AL. In an attempt to account for this potential variable, the statistical analysis controlled for AL as a covariate, hence minimising its influence on the outcomes.

CONCLUSION

Modelling of the eye with MRI provides an invaluable opportunity to investigate how eye shape and growth, both anteriorly and posteriorly, vary in myopic eyes. Observations of regional differences in anterior SAs that are modulated by refractive status suggest that structural and biomechanical changes may be evident across the anterior segment. It is unclear if these changes are an indicator or consequence of myopia, but further work is warranted to determine this. The anterior segment provides a clinically accessible site for the administration of scleral collagen cross-linking for myopia as well as surgical procedures relating to glaucoma and cataract. If refractive status affects the anatomical characteristics of the anterior eye, then improved knowledge of the optimal site for treatment is necessary. Herein, the novel application of anterior segment SA and bulbosity derived from MRI data provides an avenue for future exploration, specifically in relation to the posterior segment eye growth.

AUTHOR CONTRIBUTIONS

Hetal Buckhurst: Conceptualization (lead); data curation (lead); formal analysis (lead); funding acquisition (lead); investigation (lead); methodology (lead); project administration (lead); resources (lead); software (equal); supervision (equal); validation (equal); visualization (equal); writing – original draft (lead); writing – review and editing (lead). **Bernard Gilmartin:** Conceptualization (equal); data curation (supporting); formal analysis (equal); funding acquisition (equal); investigation (equal); methodology (equal); project administration (supporting); resources (equal); software (equal); supervision (equal); validation (equal); visualization (equal); writing – original draft (supporting); writing – review and editing (supporting). **Robert Cubbidge:** Conceptualization (supporting); data curation (supporting); formal analysis (supporting); funding acquisition (supporting); investigation (supporting); methodology (supporting); project administration (supporting); resources (supporting); software (supporting); supervision (supporting); validation (supporting); visualization (supporting); writing – original draft (supporting); writing – review and editing (supporting). **Nicola S. Logan:** Conceptualization (supporting); data curation (supporting); formal analysis (supporting); funding acquisition (lead); investigation (supporting); methodology (supporting); project administration (supporting); resources (supporting); software (supporting); supervision (supporting); validation (supporting); visualization (supporting); writing – original draft (supporting); writing – review and editing (supporting).

ACKNOWLEDGEMENTS

Hetal Buckhurst received PhD fee waiver from Aston University. Surface area was calculated using a formula developed in collaboration with Dr. Bill Cox, Aston University. Dr. Manbir Nagra is acknowledged for assistance in the MRI and biometry data collection.

FUNDING INFORMATION

This research received no specific grant from any funding agency in the public, commercial or not-for-profit sectors.

CONFLICT OF INTEREST STATEMENT

The authors report no conflicts of interest and have no proprietary interest in any of the materials mentioned in this article.

ORCID

Hetal Buckhurst https://orcid.org/0000-0002-8203-7979
Nicola S. Logan https://orcid.org/0000-0002-0538-9516

REFERENCES

1. Ohno-Matsui K, Lai TY, Lai C-C, Cheung CMG. Updates of pathologic myopia. *Prog Retin Eye Res*. 2016;52:156–87.
2. Wong TY, Ferreira A, Hughes R, Carter G, Mitchell P. Epidemiology and disease burden of pathologic myopia and myopic choroidal neovascularization: an evidence-based systematic review. *Am J Ophthalmol*. 2014;157:9–25.
3. Backhouse S, Gentle A. Scleral remodelling in myopia and its manipulation: a review of recent advances in scleral strengthening and myopia control. *Ann Eye Sci*. 2018;3:1–15.
4. McBrien N, Gentle A. Role of the sclera in the development and pathological complications of myopia. *Prog Retin Eye Res*. 2003;22:307–33.
5. Niyazmand H, Read SA, Atchison DA, Collins MJ. Effects of accommodation and simulated convergence on anterior scleral shape. *Ophthalmic Physiol Opt*. 2020;40:482–90.
6. Consejo A, Rozema JJ. In vivo anterior scleral morphometry, axial length and myopia. *Cont Lens Anterior Eye*. 2018;43:21–5.
7. Buckhurst HD, Gilmartin B, Cubbidge RP, Logan NS. In vivo measures of anterior scleral resistance in humans with rebound tonometry. *Ophthalmic Physiol Opt*. 2020;40:472–81.
8. Buckhurst HD, Gilmartin B, Cubbidge RP, Logan NS. Measurement of scleral thickness in humans using anterior segment optical coherent tomography. *PLoS One*. 2015;10:e0132902. https://doi.org/10.1371/journal.pone.0132902
9. Patel H, Gilmartin B, Cubbidge RP, Logan NS. In vivo measurement of regional variation in anterior scleral resistance to Schiotz indentation. *Ophthalmic Physiol Opt*. 2011;31:437–43.
10. Pekel G, Yagc R, Acer S, Ongun GT, Çetin EN, Simavl H. Comparison of corneal layers and anterior sclera in emmetropic and myopic eyes. *Cornea*. 2015;34:786–90.
11. Read SA, Alonso-Caneiro D, Vincent SJ, Bremner A, Fothergill A, Ismail B, et al. Anterior eye tissue morphology: scleral and conjunctival thickness in children and young adults. *Sci Rep*. 2016;6:33796. https://doi.org/10.1038/srep33796

12. Dhakal R, Vupparaboina KK, Verkicharla PK. Anterior sclera undergoes thinning with increasing degree of myopia. *Invest Ophthalmol Vis Sci*. 2020;61:6. https://doi.org/10.1167/iovs.61.4.6
13. Sung MS, Ji YS, Moon HS, Heo H, Park SW. Anterior scleral thickness in myopic eyes and its association with ocular parameters. *Ophthalmic Res*. 2021;64:567–76.
14. Consejo A, Radhakrishnan H, Iskander RD. Scleral changes with accommodation. *Ophthalmic Physiol Opt*. 2017;37:263–74.
15. Woodman-Pieterse EC, Read SA, Collins MJ, Alonso-Caneiro D. Anterior scleral thickness changes with accommodation in myopes and emmetropes. *Exp Eye Res*. 2018;177:96–103.
16. Jonas JB, Wang YA, Dong L, Guo Y, Panda-Jonas S. Advances in myopia research anatomical findings in highly myopic eyes. *Eye Vis*. 2020;7:45. https://doi.org/10.1186/s40662-020-00210-6
17. Gilmartin B, Nagra M, Logan NS. Shape of the posterior vitreous chamber in human emmetropia and myopia. *Invest Ophthalmol Vis Sci*. 2013;54:7240–51.
18. Niyazmand H, Read SA, Atchison DA, Alonso-Caneiro D, Collins MJ. Anterior scleral thickness and shape changes with different levels of simulated convergence. *Exp Eye Res*. 2021;203:108435. https://doi.org/10.1016/j.exer.2020.108435
19. Hosny M, Alio J, Claramonte P, Attia WH, Perez-Santonja JJ. Relationship between anterior chamber depth, refractive state, corneal diameter, and axial length. *J Refract Surg*. 2000;16:336–40.
20. Park SH, Park KH, Kim JM, Choi CY. Relation between axial length and ocular parameters. *Ophthalmologica*. 2010;224:188–93.
21. Gong W, Cheng T, Wang J, Zhang B, Chen J, Zhu J, et al. Role of corneal radius of curvature in early identification of fundus tessellation in children with low myopia. *Br J Ophthalmol*. 2022. https://doi.org/10.1136/bjophthalmol-2022-321295
22. Ritzmann M, Caroline PJ, Borret R, Korszen E. An analysis of anterior scleral shape and its role in the design and fitting of scleral contact lenses. *Cont Lens Anterior Eye*. 2018;41:205–13.
23. Baikoff G, Jodai HJ, Bourgeon G. Measurement of the internal diameter and depth of the anterior chamber: IOLMaster versus anterior chamber optical coherence tomographer. *J Cataract Refract Surg*. 2005;31:1722–8.
24. Werner L, Lovisolo C, Chew J, Tetz M, Müller M. Meridional differences in internal dimensions of the anterior segment in human eyes evaluated with 2 imaging systems. *J Cataract Refract Surg*. 2008;34:1125–32.
25. Geroski SH, Edelhauser HF. Transscleral drug delivery for posterior segment disease. *Adv Drug Deliv Rev*. 2001;52:37–48.
26. Zinkernagel MS, Schorno P, Eneter A, Wolf S. Scleral thinning after repeated intravitreal injections of antivascular endothelial growth factor agents in the same quadrant. *Invest Ophthalmol Vis Sci*. 2015;56:1894–900.
27. Kwok SJJ, Forawrd S, Wertheimer CM, Liapis AC, Lin HH, Kim M, et al. Selective equatorial sclera crosslinking in the orbit using a metal-coated polymer waveguide. *Invest Ophthalmol Vis Sci*. 2019;60:2563–70.
28. Wang M, Corpuz CCC, Zhang F. Shaping eyeballs by scleral collagen cross-linking: a hypothesis for myopia treatment. *Front Med*. 2021;8:655822. https://doi.org/10.3389/fmed.2021.655822
29. Ortiz S, Perez-Merino P, Duran S. Full OCT anterior segment biometry: an application in cataract surgery. *Biomed Opt Express*. 2013;4:387–96.
30. Pakuliene G, Zimarinas K, Nedzelskiene I, Siesky B, Kuzmiene L, Harris A, et al. Anterior segment optical coherence tomography imaging and ocular biometry in cataract patients with open angle glaucoma comorbidity. *BMC Ophthalmol*. 2021;21:127. https://doi.org/10.1186/s12886-021-01874-x
31. Iskander DR, Wachel P, Simpson PN, Consejo A, Jesus DA. Principles of operation, accuracy and precision of an eye surface profiler. *Ophthalmic Physiol Opt*. 2016;36:266–78.
32. Hall LA, Young G, Wolffsohn JS, Riley C. The influence of corneoscleral topography on soft contact lens fit. *Invest Ophthalmol Vis Sci*. 2011;52:6801–6.
33. Choi HJ, Lee SM, Lee JY, Lee SY, Kim MK, Wee WR. Measurement of anterior scleral curvature using anterior segment OCT. *Optom Vis Sci*. 2014;91:793–802.
34. Alonso-Caneiro D, Read SA, Vincent SJ, Collins MJ, Wojtkowski M. Tissue thickness calculation in ocular optical coherence tomography. *Biomed Opt Express*. 2016;7:629–45.
35. Stone RA, Flitcroft DI. Ocular shape and myopia. *Ann Acad Med*. 2004;33:7–15.
36. Ang M, Wong CW, Hoang QV, Cheung GCM, Lee SY, Chia A, et al. Imaging in myopia: potential biomarkers, current challenges and future developments. *Br J Ophthalmol*. 2019;103:855–62.
37. Vaught LV, Shamonin DP, Luyteb GPM, Stoel BC, Beenakker JWM. MRI-based 3D retinal shape determination. *BMJ Open Ophthalmol*. 2021;6:e000855. https://doi.org/10.1136/bmjophth-2021-000855
38. Cheng HM, Singh OS, Kwong KK, Xiong J, Woods BT, Brady TJ. Shape of the myopic eye as seen with high-resolution magnetic resonance imaging. *Optom Vis Sci*. 1992;69:698–701.
39. Atchison DA, Jones CE, Schmid KL, Pritchard N, Pope JM, Strugnell WE, et al. Eye shape in emmetropia and myopia. *Invest Ophthalmol Vis Sci*. 2004;45:3380–6.
40. Lim LS, Yang X, Gazzard G, Lin X, Sng C, Saw SM, et al. Variations in eye volume, surface area, and shape with refractive error in young children by magnetic resonance imaging analysis. *Invest Ophthalmol Vis Sci*. 2011;52:8878–83.
41. Nagra M, Gilmartin B, Thai NJ, Logan NS. Determination of retinal surface area. *J Anat*. 2017;231:319–32.
42. Nagra M, Gilmartin B, Logan NS. Estimation of ocular volume from axial length. *Br J Ophthalmol*. 2014;98:1697–701.
43. Buckhurst H, Gilmartin B, Cubbidge RP, Nagra M, Logan NS. Ocular biometric correlates of ciliary muscle thickness in human myopia. *Ophthalmic Physiol Opt*. 2013;33:294–304.
44. Chau A, Fung K, Pak K, Yap M. Is eye size related to orbit size in human subjects? *Ophthalmic Physiol Opt*. 2004;24:35–40.
45. Richdale K, Wassenaar P, Bluestein KT, Abduljalil A, Christoforidis JA, Lanz T, et al. 7 tesla MR imaging of the human eye in vivo. *J Magn Reson Imaging*. 2009;30:924–32.
46. Glarin RK, Nguyen BN, Clearly JO, Kolbe SC, Ordidge RJ, Bui BV, et al. MR-EYE: high-resolution MRI of the human eye and orbit at ultra-high field (7T). *Magn Reson Imaging Clin N Am*. 2021;29:103–16.
47. Zadnik K, Manny RE, Yu JA, Mitchell GL, Cotter SA, Quiralte JC, et al. Ocular component data in schoolchildren as a function of age and gender. *Optom Vis Sci*. 2003;80:226–36.
48. Jones LA, Mitchell GL, Mutti DO, Hayes JR, Moeschberger ML, Zadnik K. Comparison of ocular component growth curves among refractive error groups in children. *Invest Ophthalmol Vis Sci*. 2005;46:2317–27.
49. Mutti DO. Hereditary and environmental contributions to emmetropization and myopia. *Optom Vis Sci*. 2010;87:255–9.
50. Bailey MD, Sinnott LT, Mutti DO. Ciliary body thickness and refractive error in children. *Invest Ophthalmol Vis Sci*. 2008;49:4353–60.
51. Medicines and Healthcare products Regulatory Agency. Safety guidelines for magnetic resonance imaging equipment in clinical use; 2021. Available from: https://www.assets.publishing.service.gov.uk/government/uploads/system/uploads/attachment_data/file/958486/MRI_guidance_2021–4-03c. Accessed 14 Oct 2022.
52. Singh KD, Logan NS, Gilmartin B. Three-dimensional modeling of the human eye based on magnetic resonance imaging. *Invest Ophthalmol Vis Sci*. 2006;47:2272–9.
53. Consejo A, Llorens-Quintana C, Bartuzel MM, Iskander RD, Rozema JJ. Rotation asymmetry of the human sclera. *Acta Ophthalmol*. 2019;97:e266–70.
54. Marriott PJ. An analysis of global contours and haptic contact lens fitting. *Br J Physiol Opt*. 1966;23:1–40.
55. Fadel D. The influence of limbal and scleral shape on scleral lens design. *Cont Lens Anterior Eye*. 2018;41:321–8.
56. Van der Worp E. A guide to scleral fitting. Forest Grove, Oregon: Pacific University; 2010.

57. Rondeau MJ, Barcsay G, Silverman RH, Reinstein DZ, Krishnamurthy R, Chabi A, et al. Very high frequency ultrasound biometry of the anterior and posterior chamber diameter. *J Refract Surg*. 2004;20:454–64.
58. Forrester JV, Dick AD, McMenamin PG, Roberts F. The eye, basic sciences in practice. Philadelphia, Pennsylvania: Elsevier; 2008. p. 100–8.
59. Bron AJ, Tripathi RC, Tripathi BJ. Wolff's anatomy of the eye and orbit. 8th ed. London: Chapman and Hall Medical; 1997. p. 370.
60. Jonas JB, Holbach L, Panda-Jonas S. Scleral cross section area and volume and axial length. *PLoS One*. 2014;9:e93551. https://doi.org/10.1371/journal.pone.0093551
61. Van Alphen G. Choroidal stress and emmetropization. *Vision Res*. 1986;26:723–34.
62. Jonas JB, Ohno-Matsui K, Panda-Jonas S. Myopia: anatomic changes and consequences for its etiology. *Asia Pac J Ophthalmol*. 2019;8:355–9.
63. Nagra M, Gilmartin B, Logan NS, Furlong P, Wilkinson E. Conformation of sagittal and axial meridians in human myopia. *Invest Ophthalmol Vis Sci*. 2009;50:ARVO E-Abstract 3941.
64. Curtin BJ. The myopias, basic science and clinical management. Cambridge: Harper & Row; 1985. p. 200–85.
65. Greene PR, McMahon TA. Scleral creep vs. temperature and pressure in vitro. *Exp Eye Res*. 1979;29:527–37.
66. Shunmugam M, Shah AN, Hysi PG, Williamson TH. The pattern and distribution of retinal breaks in eyes with rhegmatogenous retinal detachment. *Am J Ophthalmol*. 2014;157:221–6.
67. Grzybowski A, Eppig T. Angle alpha as predictor for improving patient satisfaction with multifocal intraocular lenses? *Graefes Arch Clin Exp Ophthalmol*. 2021;259:563–5.
68. Mahr MA, Simpson MJ, Erie JC. Angle alpha orientation and magnitude distribution in a cataract surgery population. *J Cataract Refract Surg*. 2020;46:372–7.

How to cite this article: Buckhurst H, Gilmartin B, Cubbidge R, Logan NS. Conformation of the anterior segment in human myopia. *Ophthalmic Physiol Opt*. 2023;00:1–9. https://doi.org/10.1111/opo.13095